Title: Improvement of separation performance by fluid motion in the membrane module with a helical baffle

Authors: Takaaki Akagi[a], Takafumi Horie[a, b,*], Hayato Masuda[c], Keigo Matsuda[d], Hideyuki Matsumoto[e], Naoto Ohmura[a], Yushi Hirata[f]

[a] Department of Chemical Science and Engineering, Graduate School of Engineering, Kobe University

1-1 Rokkodai, Nada, Kobe, Hyogo 657-8501, Japan

[b] Center for Membrane and Film Technology, Graduate School of Engineering, Kobe University

1-1 Rokkodai, Nada, Kobe, Hyogo 657-8501, Japan

[c] School of Food and Nutritional Science, University of Shizuoka

52-1 Yada, Suruga, Shizuoka 422-8526, Japan

[d] Department of Chemistry and Chemical Engineering, Graduate School of Science and Engineering, Yamagata University

4-3-16, Jonan, Yonezawa, Yamagata 992-8510, Japan

[e] Renewable Energy Research Center, National Institute of Advanced Industrial Science and Technology (AIST),

2-2-9, Machiikedai, Koriyama, Fukushima 963-0298, Japan

[f] Graduate School of Engineering Science, Osaka University

1-3 Machikaneyama, Toyonaka, Osaka 560-8531, Japan

*Corresponding author

E-mail address: horie@dragon.kobe-u.ac.jp

Abstract

Pressure-driven membrane filtration processes such as microfiltration and ultrafiltration are still hindered by concentration polarization and membrane fouling. Generally in these filtration processes, concentration polarization causes decline of permeate flux and rejection, and fouling leads to permeate flux decline with the increase of rejection. The use of high shear stress for cross flow filtrations has long been considered one of the most efficient methods for overcoming these problems. However, circumferential fluid motion of the hollow fiber membrane surface is also important to avoid formation of a high concentration layer on the surface. In this study, ultrafiltration of humic acid aqueous solution using a polyethersulfone hollow fiber membrane was selected as a model case, and a membrane module with a helical baffle installed around the membrane was used. With the insertion of the baffle, normalized permeate flux and rejection became higher than those without the baffle at the wide range of the feed flow rate. In order to identify the cause of the improvement, CFD simulation was conducted for different baffle geometries. Swirling flow motion generated by the helical baffle around the membrane became more dominant with the lower aperture ratio of the cross sectional area, and there existed the optimum value for the swirling flow generation in terms of the variation of the helical baffle pitch length. The intensity of this fluid motion was characterized by Swirl number and it was found out that high separation performance was obtained at the high Swirl number.

Keywords: ultrafiltration; water purification; swirling flow, helical coil; process intensification

1. Introduction

Membrane filtration is applied to a wide variety of industrial fields, such as wastewater, food, pharmaceutical and petrochemical processing and so on. Among these, pressure-driven processes such as microfiltration and ultrafiltration have been still seriously hindered by concentration polarization and membrane fouling. Some of the components in the solution are rejected by the membrane, and the rejected components are concentrated at the upstream membrane surface. This is called concentration polarization which is often the reason for the serious limitation due to its negative influence on the transmembrane flux in microfiltration and ultrafiltration. Furthermore, the emergence of concentration gradient at the membrane and solution interface promotes the transfer of the rejected components through the membrane and results in the decrease in the separation performance. Fouling is often the result of concentration polarization and could be described as adsorption on pore walls or accumulation of foulant to form a second layer on the membrane surface which causes the decline of permeate flux [1]. However, with the increase of the resistance to the flux, the fouling also leads to the increase of the ability to reject the foulant due to the pore capacity decline or cake layer formation.

Hollow fiber membrane filtration is mostly carried out in a cross-flow manner because the axial fluid flow along the membrane surface increases mass transfer from the membrane surface to the bulk solution. This mass transfer improvement reduces the concentration of the concentration polarization layer at the membrane surface and thus inhibits the fouling formation as a result of the concentration polarization [1]. In addition, the axial flow generates shear stress at the vicinity of the membrane surface and is capable of removing the membrane fouling. Generally the flow rate of the processing fluid is quite high and the flow regime is turbulent to enhance the mass transfer and shear stress. This simple method is widely employed in industry but contains a problem that the high flow rate causes the pressure drop increment leading to the high power consumption. However, there are also reports about inhibition of declines in performance by utilizing fluid motion such as vortex and periodic unsteady flow; applications of Taylor vortices [2], Dean vortices [3] and oscillating motions [4, 5].

The use of baffles in a tube is a simple way to induce specific flow fields [6-12]. Wide variety of baffle configurations has been tested such as central baffles [10], rod baffles [11] and helical baffles [6-9]. With regard to the helical baffle, the flow visualization [13] and the effect of heat transfer by changing baffle geometry were carried out experimentally [14]. It was also shown that the performance for membrane filtration was improved and greatly affected by the baffle geometry inserted into the membrane tube [6, 7]. The effects of feed concentration, net flow rate and transmembrane pressure were investigated by flow analysis using CFD in the membrane module with a helical baffle [8, 9], but the investigations in terms of the systematic changes of the baffle geometries were not carried out, or in other words they focused on the comparison of the cases with and without baffles. In addition, these studies were conducted under turbulent flow regime based on the standard operational condition [7-12]. Therefore, the flow patterns are so complex that a specific flow motion affecting on the improvement the filtration performance haven't been sufficiently described.

In order to realize more efficient filtration processes, operation at a low flow rate is required from the aspects of low pressure drop or power consumption. By utilizing a specific fluid motion induced by a helical baffle high permeate flux and rejection can be achieved under low flow rate condition. In this study a cross-flow-type membrane module with a helical baffle around a hollow fiber membrane was employed and the relationship between fluid motion and filtration performance was investigated experimentally and numerically to identify the cause of the performance improvement.

2. Materials and methods

2.1. Experimental setup and filtration medium

Fig. 1 shows the experimental setup for ultrafiltration. A polyethersulfone (PES) hollow fiber membrane (molecular weight cut off (MWCO) = 150 kDa; inner diameter = 0.80 mm; outer diameter = 0.95 mm; length = 110 mm; effective surface area 3.3×10^{-4} m^2) purchased from Daicen Membrane-Systems LTD. (Product No. FUS1582) was installed concentrically in a clear acrylic resin pipe with a

4 mm inner diameter. The membrane is asymmetric but has skin layers for filtration on the inner and outer sides [15]. A helical baffle made of a bronze wire was inserted into the gap between the membrane and the resin pipe. As for the water purification experiment, humic acid, a major contaminant of drinking water, was selected as a model filtrated component in this study. The concentration of humic acid in the aqueous solution was fixed at 50 mg·L^{-1}, and pH was adjusted to 8.4 by adding sodium hydrogen carbonate to be 1 mM. Each filtration experiment was carried out by forcing a feed solution to permeate from the outside to the inside of the hollow fiber membrane by 0.5 bar transmembrane pressure.

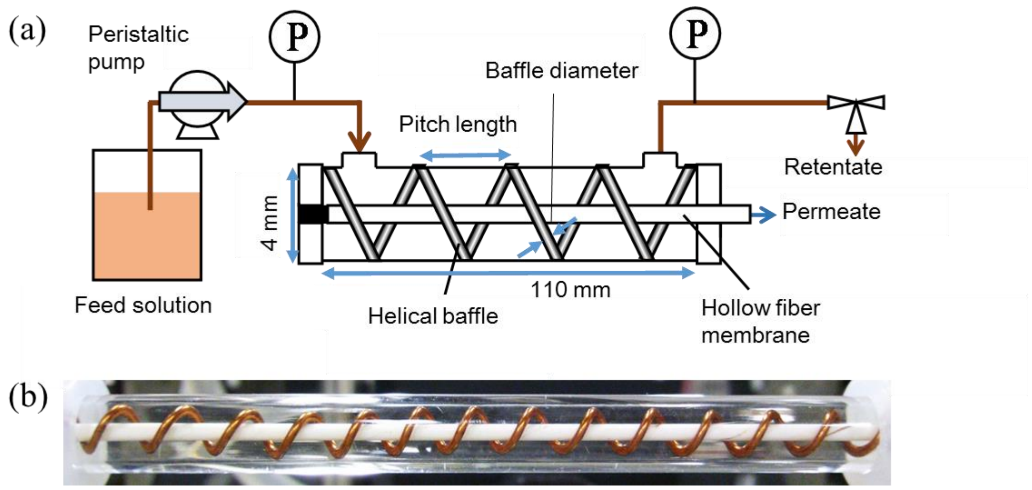

Fig. 1 (a) Schematic of the external-pressure-type cross flow filtration module with a hollow fiber membrane and a helical baffle. (b) Picture of the membrane module with a helical baffle

2.2. Evaluated experimental conditions

An aperture ratio of the open cross-sectional area of the module, Φ [%], and a baffle pitch length, b [m], were varied at 27, 34 and 53 %, and 2 – 12 mm, respectively. The aperture ratio can be varied by changing the diameter of the baffle wires and calculated by subtracting the projected areas of the membrane and helical baffle from the cross sectional area of the module. The baffle pitch length is a distance between the coils. The inner diameter of the module, d_m [m], was fixed at 4 mm, and the baffle pitch was normalized by being divided by d_m. The effect of Reynolds number, *Re*, was also examined by changing the flow rate of the feed solution. All of the examined experimental conditions are listed in Table 1.

Table 1 Experimental conditions and geometric dimensions of helical baffles

Reynolds number *Re* [-]	Pitch length *b* [mm]	Tube diameter d_m [mm]	Baffle diameter d_b [mm]	Aperture ratio Φ [%]	Trans membrane pressure [bar]
68 – 615	2 – 12	4	0.5, 0.85, 1.0	53, 34, 27	0.5

2.3 Methods to determine permeate flux and humic acid concentration

A permeability was evaluated by a normalized permeate flux, J/J_0 to eliminate the individual membrane variability. J and J_0 were permeate fluxes when the humic acid solution and distilled water were processed, respectively. Samples permeated through the membrane and dripping out from the one side of the membrane were collected and weighed to determine a permeate flux. A separation performance was represented by rejection, $R = 1 - (C/C_0)$ where C and C_0 are the concentrations of humic acid in the permeated samples and the feed solution, respectively. This is not an intrinsic rejection but an observed rejection. The concentration was determined by measuring absorbance at 254 nm light [16] using a UV-vis spectrophotometer, SHIMADZU MPS-2400.

2.4. Numerical simulation of fluid motion in the membrane module

The numerical simulation was conducted using commercial CFD software, (R-flow, RFLOW Co. Ltd.) in order to observe the flow field in the module. The permeation through the membrane and transmembrane pressure were not considered in the calculation because the permeate flux was much lower than that of the feed flow. The geometry of the module used for the simulation was the same as the experiment shown in Fig. 1 and Table 1, and the properties of the fluid were assumed to be the same as water. The walls of the membrane surface, the inner surface of the cylinder and the outer surface of the helical baffle were considered to be non-slip condition. The pressure-velocity-coupling scheme was resolved with SIMPLE algorithm. Mesh was 24 in the radial direction, 1700 in the axial direction and 100 in the circumference direction. The governing equations used for the simulation are the conservation equations of momentum and mass are given as

$$\frac{\partial \boldsymbol{u}}{\partial t} + (\boldsymbol{u} \cdot \nabla)\boldsymbol{u} = -\frac{\nabla p}{\rho} + \frac{1}{\rho}\nabla \cdot (\eta \nabla \boldsymbol{u}) + \boldsymbol{g} \tag{1}$$

$$\nabla \cdot \boldsymbol{u} = 0 \tag{2}$$

where $\boldsymbol{u}$ is the fluid velocity, t is the time, p is the pressure, ρ is the density, η is the viscosity and $\boldsymbol{g}$ is the gravitational acceleration. In this simulation, the steady state was assumed. The validation of the simulation and mesh sizes were conducted by comparing the pressure drops of the simulation results and experimental results.

3. Results and discussion

3.1 Determination of fouling mechanism

In order to examine the effect of fluid motion on fouling removal, it is necessary to comprehend the mechanism of the fouling deposition on the membrane surface in advance. Table 2 shows the list of the filtration rate equations expressing the 4 different blocking filtration models under constant pressure condition [17]. In the equations, $(\mathrm{d}v/\mathrm{d}\theta)_0$ is the initial filtration rate and K_{cb}, K_{sb}, K_{ib} and K_{c} are constants for each model. These equations are originally from the equation (3)

$$\frac{\mathrm{d}^2\theta}{\mathrm{d}v^2} = k_{\mathrm{p}}\left(\frac{\mathrm{d}\theta}{\mathrm{d}v}\right)^n \tag{3}$$

where θ is a filtration time, v is a cumulative filtrate volume per unit effective membrane area, k_{p} and n are constants. n can be determined corresponding to each model as shown in Table 2. The schematic diagrams of these models were presented in the papers [17-19]. (a) is a complete-blocking model: Particles larger than the membrane pores uniformly block pores on the membrane surface. (b) is a standard-blocking model: Particles smaller than the membrane pores deposit on the wall of the pores and the pore capacity gradually decreases. (c) is an intermediate-blocking model: This is similar in that particles larger than the membrane pores uniformly block. Most of the pores are blocked at the initial stage while a lot of open pores exist, but as the blocking proceeds it becomes more difficult for this to occur due to the reduced number of pores. In order to describe the process, the model equation was constructed by Hermia (1982) based on a stochastic model [20]. (d) is a cake filtration. It is not pore blocking but cake formation on the membrane surface, and the filtration resistance increases gradually by the cake formation and its growth on the membrane surface. Although these 4 processes may occur simultaneously, the most dominant blocking mechanism can be determined by conducting the linear plotting of experimental data in accordance with the model equations.

Table 2 Filtration rate equations under constant pressure condition for various blocking filtration models [17]

Blocking filtration law	*n*	Filtration rate equation
(a) Complete blocking	2	$\frac{\mathrm{d}v}{\mathrm{d}\theta}=\left(\frac{\mathrm{d}v}{\mathrm{d}\theta}\right)_0-K_{\mathrm{cb}}v$
(b) Standard blocking	1.5	$\frac{\mathrm{d}v}{\mathrm{d}\theta}=\left(\frac{\mathrm{d}v}{\mathrm{d}\theta}\right)_0\left(1-\frac{K_{\mathrm{sb}}v}{2}\left(\frac{\mathrm{d}v}{\mathrm{d}\theta}\right)_0^{-1/2}\right)^2$
(c) Intermediate blocking	1	$\frac{\mathrm{d}v}{\mathrm{d}\theta}=\left(\frac{\mathrm{d}v}{\mathrm{d}\theta}\right)_0\exp\left(-K_{\mathrm{ib}}v\right)$
(d) Cake filtration	0	$\frac{\mathrm{d}\theta}{\mathrm{d}v}=\left(\frac{\mathrm{d}\theta}{\mathrm{d}v}\right)_0+K_{\mathrm{c}}v$

Fig. 2 shows the experimental results modified with each of the model equations when the humic acid solution and polyethersulfone membrane were used without baffles. Each coefficient of determination was compared in the wide range of the cumulative filtrate volume per unit effective membrane area, v [$\mathrm{m^3 \cdot m^{-2}}$]. The value for the cake filtration was the closest to 1 compared with the other 3 cases, and thus the cake filtration turned out to be a dominant model. This indicates that most of the foulant particles accumulated on the membrane surface. There are two possibilities to inhibit concentration polarization and fouling thus maintaining high filtration performance. The first is the removal of deposited foulant particles by a high shear stress due to a high flow rate. The other is to generate a flow which keeps foulant particles away from the membrane surface by replacing the fluid at the surface.

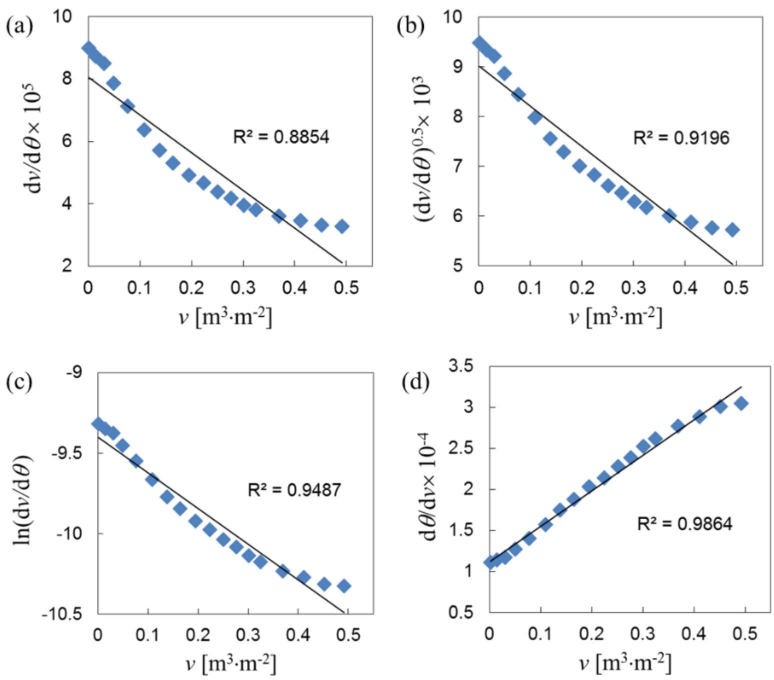

Fig. 2 Linear fitting results with the 4 different filtration blocking models listed in Table 2 when the humic acid and polyethersulfone membrane were used.

3.2 Time variation of permeate flux and rejection

Fig. 3 shows that time variation of permeate flux and rejection for the cases without and with a baffle (Re = 68, b/d_m = 1.5, Φ = 34%). Only by inserting the helical baffle, the permeate flux and rejection were improved from the initial filtration time. As for the cake filtration mechanism, foulant is considered to be concentrated quickly on the membrane surface because the permeate flux is higher at the initial stage. The concentrated foulant passes through the membrane with the driving force of the concentration gradient at the membrane and solution interface (i.e. concentration polarization) and causes the rejection decrease as a result. The rejection for the case with the helical baffle was much higher at the initial stage and kept higher value than that without the baffle. It indicates that the specific fluid motion induced by the helical baffle promoted mixing at the vicinity of the membrane surface and kept the foulant away from this region. In addition, the permeate flux also kept at higher value than that without the baffle. Since it is assumed that the cake layer leading to the permeate flux reduction might be formed after the concentrated foulant was adsorbed and accumulated on the membrane surface, the mixing of the high concentrated region inhibited the formation of the cake layer as well and led to the preservation of higher permeate flux.

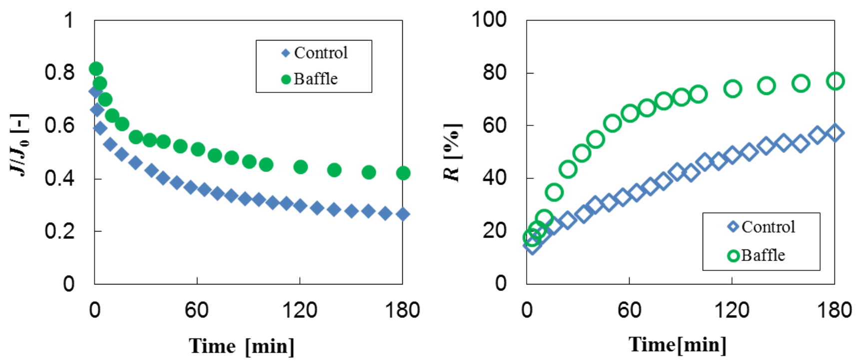

Fig. 3 Time variation of the normalized permeate flux J/J_0 and rejection R for the membrane module with the helical baffle (Baffle) and without the helical baffle (Control) under the condition Re = 68, b/d_m = 1.5 and Φ = 34 %.

3.3 Effect of Reynolds number on filtration performance

Fig. 4 shows the permeate flux and rejection against Reynolds number for the cases without and with the helical baffle (b/d_m = 1.5, Φ = 34%). Each of the plots was obtained at 180 min when the time variations of the permeate flux and rejection were considered to be stable, but it should be note that it didn’t reach the inherent steady state. As for the case without the baffle, both of the permeate flux and rejection increased with Reynolds number increase. When the flow rate becomes higher, the mass transfer from the membrane surface of the feeding side can be promoted and leads to the reduction of the concentration polarization layer. This reduction of the concentration gradient between the feeding and permeation sides of the membrane resulted in the rejection increment with the mechanism explained in the previous section. Besides, in the case of pressure driven processes, concentration gradient between the feeding and permeation sides of the membrane causes an increase of the osmotic pressure gradient in the membrane, which reduces the net driving pressure gradient [21]. The reduction of the layer thickness also increased the permeate flux by reducing this osmotic pressure. Another cause of the permeate flux increment was the high shear stress removing the accumulated foulant on the membrane surface and maintaining the cake layer thinner. However, the flux and rejection improvement became lower at the higher flow because the streamlines were uniform along the axial direction of the membrane fiber, and even when the flow rate became higher, concentration polarization layer still existed to some extent which caused fouling development.

On the other hand, for the case with the helical baffle, higher filtration performance was obtained at the low Reynolds number. Even when the case with the baffle at Re = 68 and the case without the baffle at Re = 615 were compared, the former showed higher filtration performance. This is because the specific fluid motion induced by the helical baffle gave a disturbance on the concentration polarization layer, and led to the reduced concentration. Additionally, since the highly concentrated region was difficult to be formed on the surface, the less amount of foulant could be adsorbed and accumulated. Thus the thick cake layer was not formed and the high permeate flux could be achieved. It is inferred that the specific fluid motion generated by the guide of the helical baffle was more effective on maintaining the high filtration performance than the high flow rate.

However, in the case with the helical baffle, the degree of the improvement obtained by the flow rate (Re) increase was less than the case without the baffle. Although the major cause of the high performance at the low flow rate was the fluid motion induced by the helical baffle, the proportion of the by-pass flow passing through the gap between the baffle and membrane would be increased when the flow rate was higher. In other words, the fluid motion induced by the baffle became less dominant at the higher flow rate.

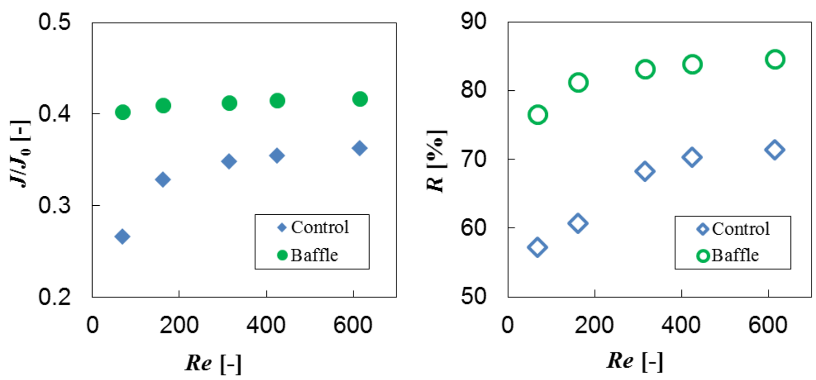

Fig. 4 Dependency of Reynolds number on the normalized permeate flux J/J_0 and rejection R for the membrane module with the helical baffle (B) and without the helical baffle (C) under the condition $b/d_m = 1.5$ and $\Phi = 34$ % after the 180 min filtration operation.

3.4 Numerical analysis of fluid motions with different baffle geometries

In order to identify the specific fluid motion induced by the helical baffle and enhancing the filtration performance, the numerical investigation was carried out. Fig. 5 shows (a) the streamlines starting from the randomly selected initial positions and (b) the contour of the circumferential flow velocity to the counterclockwise direction in the cross section at the aperture ratios, $\Phi = 27\%$ and 53% with the fixed pitch length of the helical baffle ($b/d_m = 1.5$). It should be noted that (a) the dots on the baffle have no meaning and (b) the violet areas at the center and at the lower right are the membrane without considering the hollow space and the cross-section of helical baffle, respectively. At the lower aperture ratio, it was clearly seen that the streamlines had the similar trajectory as the geometry of the helical baffle. Additionally, high velocity region above the baffle in the circumferential velocity field could be observed. This specific fluid motion induced by the helical baffle is called as “swirling flow” in the following. When the higher aperture ratio of 53%, the swirling flow became less dominant compared with the axial component because the flow passed though the gap more easily.

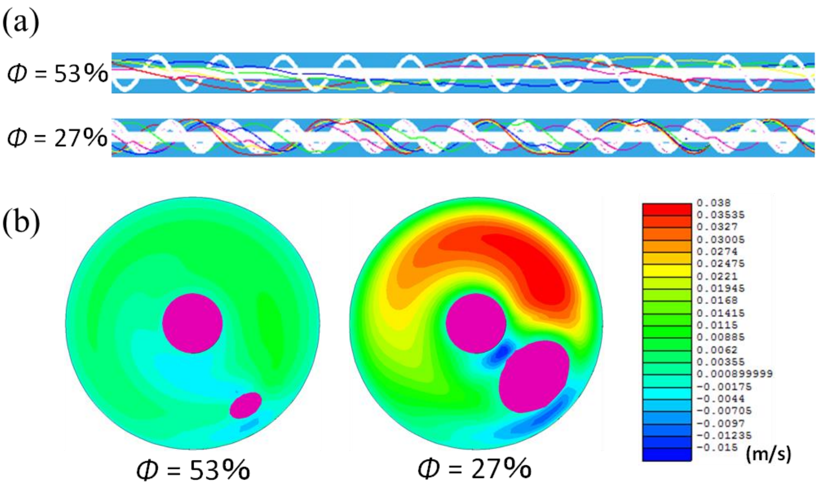

Fig. 5 (a) Streamlines starting from the randomly selected initial positions and (b) circumferential velocity fields in the cross section at the aperture ratios, Φ = 27% and 53% under the condition Re = 68 and b/d_m = 1.5.

Fig. 6 also shows the streamline and the circumferential flow velocity in the cross section when the normalized pitch, b/d_m, were 1.0, 1.5 and 3.0 and the aperture ratio was constant at 38%. The number of wire coils around the membrane was adjusted by changing the pitch length. At the lower b/d_m, (i.e. more coils around the membrane), the streamline was predominantly axial, and swirling or rotational movement was weak. Conversely, at a higher b/d_m, the number of the rotations of the streamline was nearly equal to the coils of the helical baffle. In comparison of 1.5 b/d_m, and 3 b/d_m, coil rates, the streamline completed more rotations at 1.5 b/d_m. Also, when examining the circumferential velocity, a higher velocity region above the baffle was observed at 1.5 b/d_m, although there was not a significant difference. This shows that in order to maximize the number of rotations and rotation velocity of the fluid, there exists an optimum b/d_m.

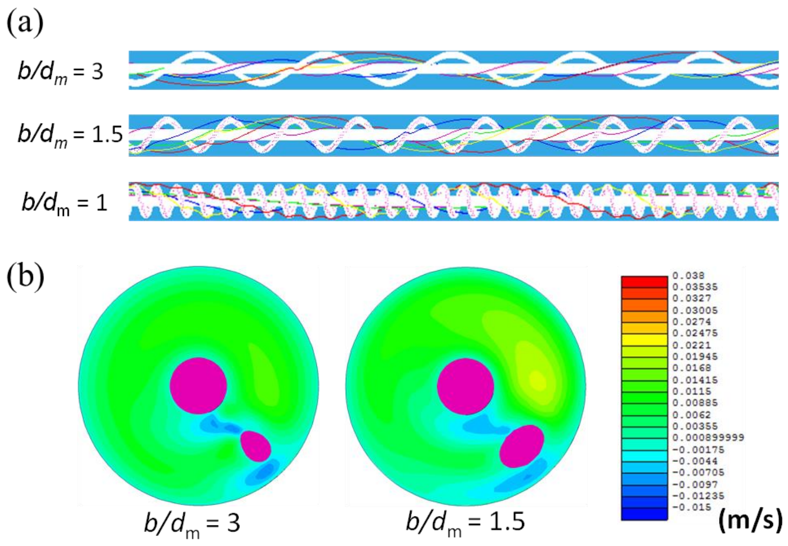

Fig. 6 (a) Streamlines starting from the randomly selected initial positions and (b) circumferential velocity fields when the normalized pitch b/d_m were 1.0, 1.5 and 3.0 under the condition Re = 68 and Φ = 38%.

3.5 Evaluation of performance using Swirl number

Figs. 7 and 8 show the permeate flux and rejection when the aperture ratio was changed at the constant b/d_m and when the b/d_m was changed at the constant aperture ratio, Φ, respectively. In Fig. 7, the lower the aperture ratio became, the higher permeate flux and rejection were achieved. The lower aperture ratio corresponds to the narrower gap between the baffle and the other surfaces and made the swirling flow stronger due to the reduction of the by-pass flow as shown in the previous section. The swirling flow generated the flow which was not parallel to the membrane surface, and this non-parallel flow might cause the mixing effect on the concentration polarization layer to decrease the concentration at the membrane surface even under the laminar flow condition. Additionally, since the fouling was formed as a result of the concentration polarization layer, the fouling was also suppressed and the permeate flux showed a better performance at the low aperture ratio. In Fig. 8, the lower b/d_m caused the by-pass flow because it made more difficult to flow along the helical baffle, and thus led to the less number of the rotations of the streamline. Additionally, at the higher b/d_m, the number of the helical baffle coils per unit length of the membrane was less, and the number of the rotations of the streamline necessarily became less even though the by-pass flow was suppressed. Therefore, the permeate flux showed the optimum value around b/d_m = 1.5. On the other hand, the decreasing tendencies in the rejection at the lower b/d_m and at the higher b/d_m were less obvious than the case in Fig. 7. It might be said that the circumferential velocity was lower than the case in Fig. 7 and could not suppress the cake layer formation on the membrane surface, and this thicker cake layer also rejected the foulant to increase the rejection. However, the mechanisms of the disturbance for the concentration layer and cake layer were not elucidated sufficiently and further investigation would be required.

The swirling flow induced by the helical baffle could reduce the formation of the concentration polarization and cake layer rather than the high shear stress. Swirl number, m [-], was employed in order to evaluate both of the effects of flow rate and the baffle geometry. This dimensionless number is defined as the ratio of the axial flux of angular momentum to the axial flux of axial momentum [22]. It was originally proposed by Chigier and Beer [23] and simplified by Sheen et al. [24]. This represents the intensity of the swirling flow.

$$m = \frac{\int_0^{R_\mathrm{i}} \rho U V r \, 2\pi r dr}{R_\mathrm{i} \int_0^{R_\mathrm{i}} \rho U^2 \, 2\pi r dr} = \frac{\int_0^{R_\mathrm{i}} U V r^2 dr}{R_\mathrm{i} \int_0^{R_\mathrm{i}} U^2 r \ \ d} \tag{4}$$

where r [m] is a radial position, R [m] is a tube radius, U [m·s^{-1}] is a axial fluid velocity, V [m·s^{-1}] is a circumferential fluid velocity and ρ [kg·m^{-3}] is a fluid density. The velocity components were obtained from the results of the CFD simulation in the section 3.4. Fig. 9 shows the relationship between Swirl number and the filtration performance. The permeate flux and rejection was raised with Swirl number increase. It is assumed that the high mixing intensity could be obtained due to the swirling motion of fluid at high Swirl number and inhibited the formation of high concentrated layer at the membrane surface. It is concluded that the filtration performance was improved by enhancing the intensity of swirling motion in the membrane module.

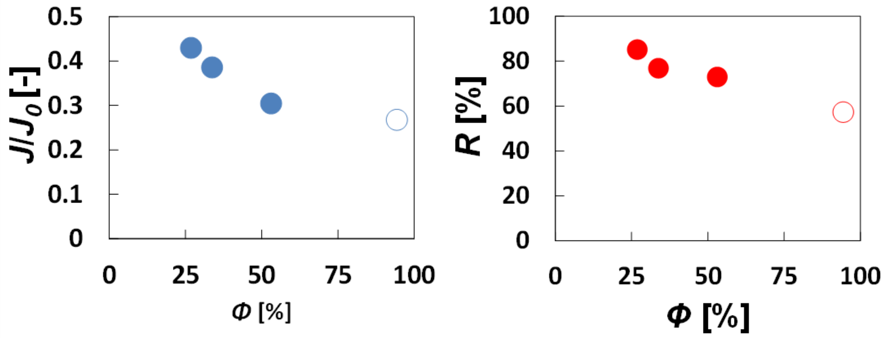

Fig. 7 Effect of the aperture ratio on the normalized permeate flux J/J_0 and rejection R after the 180 min operation under the condition Re = 68 and b/d_m = 1.5 and the hollow marks indicates the results without the baffle.

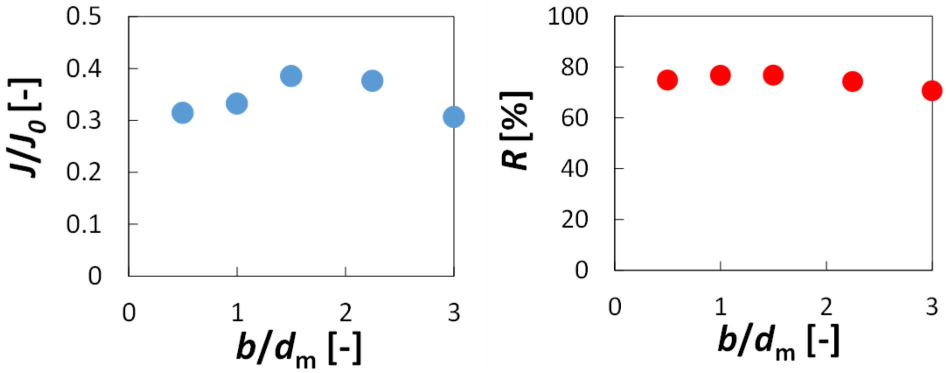

Fig. 8 Effect of the aperture ratio on the normalized permeate flux J/J_0 and rejection R after the 180 min operation under the condition Re = 68 and Φ = 34% and the hollow marks indicates the results without the baffle.

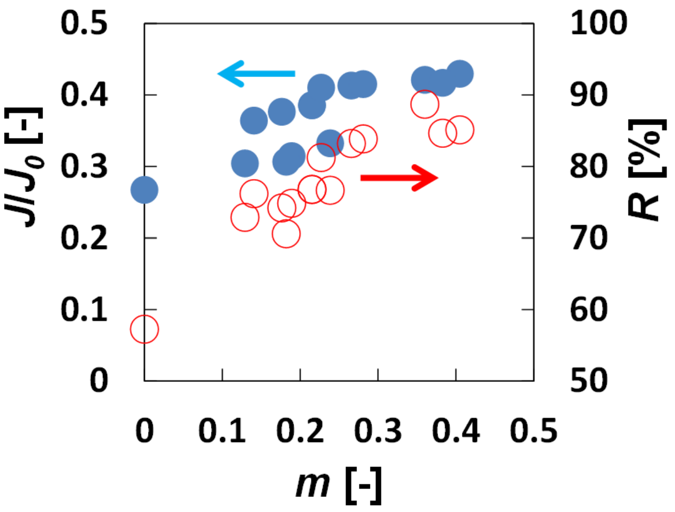

Fig. 9 Dependency of Swirl number on the filtration performance after 180 min operation: Filled and hollow marks represent the normalized permeate flux J/J_0 and rejection R respectively.

4. Conclusion

The effect of fluid motion on the filtration performance was investigated for the membrane module with the helical baffle. Humic acid solution and polyethersulfone membrane were used for the model filtration process, and the dominant fouling mechanism model was determined to be cake filtration. With the helical baffle, the filtration performance became higher even at the low flow rate of the processing fluid than that without the baffle. Swirling flow induced by the helical baffle was more effective for suppressing concentration polarization and fouling than high flow rate such as turbulent flow. The swirling flow has a characteristic flow pattern to increase the mixing effect around the membrane surface and reduce the deposition of the foulant. As the intensity of the swirling flow was characterized by the dimensionless number, Swirl number, the concentration and deposition of the foulant were reduced and the filtration performance was improved with the Swirl number increase.

Acknowledgments

A part of this work has been supported by Kawanishi Memorial Shin Meiwa Education Foundation.

The authors wish to thank Mr. Norihisa Kumagai for his experimental support.

Nomenclature

b	pitch of helical baffles (m)
C	concentrations of humic acid in the permeate (kg m^{-3})
C_0	concentrations of humic acid in the feed solution (kg m^{-3})
d_m	inner diameter of the module cylinder (m)
g	gravitational acceleration (m s^{-2})
J	permeate flux (m^3 m^{-2} s^{-1})
J_0	pure water permeate flux (m^3 m^{-2} s^{-1})
k_p	constant in Eq.(3) (m^{n-2} s^{1-n})
K_cb	constant in Table 2 (s^{-1})
K_sb	constant in Table 2 (m$^{-1/2}$ s$^{-1/2}$)
K_ib	constant in Table 2 (m^{-1})
K_c	constant in Table 2 (s m^{-2})
m	Swirl number (-)
n	constant in Eq.(3) (-)
p	pressure (Pa)
r	radial position (m)
R	rejection (%)
R_i	inner radius of the membrane module cylinder (m)
t	time (s)
u	fluid velocity (m s^{-1})
U	axial fluid velocity (m s^{-1})
v	cumulative filtrate volume per unit effective membrane area (m^3 m^{-2})

V circumferential fluid velocity (m s^{-1})

Greek letters

Φ aperture ratio of the open cross-sectional area (%)

ρ fluid density (kg m^{-3})

μ viscosity (Pa s)

θ filtration time (s)

References

[1] M. Mulder, Basic Principles of Membrane Technology, second ed., Kluwer Academic Publishers, Netherlands, 1997.

[2] K.H. Kroner, V. Nissinen, Dynamic filtration of microbial suspensions using an axially rotating filter, Journal of Membrane Science 36 (1988) 85-100. http://dx.doi.org/10.1016/0376-7388(88)80009-7

[3] C. Guigui, P. Manno, P. Moulin, M.J. Clifton, J.C. Rouch, P. Aptel, J.M. Laîné, The use of Dean vortices in coiled hollow-fibre ultrafiltration membranes for water and wastewater treatment, Desalination 118 (1998) 73-80. http://dx.doi.org/10.1016/S0011-9164(98)00089-7

[4] A. Kola, Y. Ye, A. Ho, P. Le-Clech, V. Chen, Application of low frequency transverse vibration on fouling limitation in submerged hollow fibre membranes, Journal of Membrane Science 409-410 (2012) 54-65. http://dx.doi.org/10.1016/j.memsci.2012.03.017

[5] H.G. Gomaa, S. Rao, A.M. Al-Taweel, Intensification of membrane microfiltration using oscillatory motion, Separation and Purification Technology 78 (2011)336-344. http://dx.doi.org/10.1016/j.seppur.2011.01.007

[6] B.B. Gupta, J.A. Howell, D. Wu, R.W. Field, A helical baffle for cross-flow microfiltration, Journal of Membrane Science 102 (1995) 31-42. http://dx.doi.org/10.1016/0376-7388(94)00241-P

[7] A.L. Ahmad, A. Mariadas, Baffled microfiltration membrane and its fouling control for feed water of desalination, Desalination 168(2004) 223-230. http://dx.doi.org/10.1016/j.desal.2004.07.002

[8] S. Popović, D. Jovičević, M. Muhadinović, S. Milanović, M. N. Tekić, Intensification of microfiltration using a blade-type turbulence promoter, Journal of Membrane Science 425-426 (2013) 113-120. http://dx.doi.org/10.1016/j.memsci.2012.09.032

[9] Y. Liu, G. He, L. Ding, H. Dou, J. Ju, B. Li, Experimental and CFD studies on the performance of microfiltration enhanced by a turbulence promoter, Chinese Journal of Chemical Engineering 20(4) (2012) 617-624. http://dx.doi.org/10.1016/S1004-9541(11)60226-7

[10] Y. Liu, G. He, X. Liu, G. Xiao, B. Li, CFD simulations of turbulent flow in baffle-filled membrane tubes, Separation and Purification Technology 67 (2009) 14-20. http://dx.doi.org/10.1016/j.seppur.2009.02.022

[11] S. Ahmed, M. T. Seraji, J. Jahedi, M.A. Hashib, CFD simulation of turbulence promoters in a tubular membrane channel, Desalination 276 (2011) 191-198. http://dx.doi.org/10.1016/j.desal.2011.03.045

[12] S. Ahmed, M. T. Seraji, J. Jahedi, M.A. Hashib, Application of CFD for simulation of a baffled tubular membrane, Chemical Engineering Research and Design 90 (2012) 600-608. http://dx.doi.org/10.1016/j.cherd.2011.08.024

[13] A. García, J.P. Solano, P.G. Vicente, A. Viedma, Flow pattern assessment in tubes with wire coil inserts in laminar and transition regimes, International Journal of Heat and Fluid Flow 28 (2007)

516-525.
http://dx.doi.org/10.1016/j.ijheatfluidflow.2006.07.001
[14] A. García, P. G. Vicente, A. Viedma, Experimental study of heat transfer enhancement with wire coil inserts in laminar-transition-turbulent regimes at different Prandtl numbers, International Journal of Heat and Mass Transfer 48 (2005) 4640-4651.
http://dx.doi.org/10.1016/j.ijheatmasstransfer.2005.04.024
[15] F. Razi, I. Sawada, Y. Ohmukai, T. Maruyama, H. Matsuyama, The improvement of antibiofouling efficiency of polyethersulfone membrane by functionalization with zwitterionic monomers, Journal of Membrane Science 401–402 (2012) 292–299.
http://dx.doi.org/10.1016/j.memsci.2012.02.020
[16] W. Yuan, A.L. Zydnety, Humic acid fouling during microfiltration, Journal of Membrane Science 157 (1999) 1–12.
http://dx.doi.org/10.1016/S0376-7388(98)00329-9
[17] E. Iritani, Modeling and evaluation of pore clogging of membrane in membrane filtration (in Japanese), Kagaku Kogaku Ronbunshu 35(1) (2009) 1–11.
http://dx.doi.org/10.1252/kakoronbunshu.35.1
[18] B. Blankert, B.H.L. Betlem, B. Roffel, Dynamic optimization of a dead-end filtration trajectory: Blocking filtration laws, Journal of Membrane Science 285 (2006) 90–95.
http://dx.doi.org/10.1016/j.memsci.2006.07.044
[19] I. Sutzkover-Gutman, D. Hasson, R. Semiat, Humic substances fouling in ultrafiltration processes, Desalination 261 (2010) 218–23.
http://dx.doi.org/10.1016/j.desal.2010.05.008
[20] J. Hermia, Constant Pressure Blocking Filtration Laws—Application to power-law non-Newtonian fluids, Transactions of the Institution of Chemical Engineers 60 (1982) 183–187.
[21] R.W. Baker, Membrane Technology and Applications, third ed., John Wiley & Sons, 2012.

[22] A. K. Gupta, D. G. Lilley, N. Syred, Swirl flows, first ed., Routledge, London, 1984.

[23] N. A. Chigier and J. M. Beér, Velocity and Static-Pressure Distributions in Swirling Air Jets Issuing From Annular and Divergent Nozzles, Journal of Basic Engineering 86, (1964) 788-796. http://dx.doi.org/10.1115/1.3655954

[24] H.J. Sheen, W.J. Chen, S.Y. Jeng, T.L. Huang, Correlation of swirl number for a radial-type swirl generator, Experimental Thermal and Fluid Science 12 (1996) 444-451. https://doi.org/10.1016/0894-1777(95)00135-2